



CHORUS

This is the accepted manuscript made available via CHORUS. The article has been published as:

Type-II Symmetry-Protected Topological Dirac Semimetals

Tay-Rong Chang, Su-Yang Xu, Daniel S. Sanchez, Wei-Feng Tsai, Shin-Ming Huang, Guoqing Chang, Chuang-Han Hsu, Guang Bian, Ilya Belopolski, Zhi-Ming Yu, Shengyuan A. Yang, Titus Neupert, Horng-Tay Jeng, Hsin Lin, and M. Zahid Hasan

Phys. Rev. Lett. **119**, 026404 — Published 14 July 2017

DOI: [10.1103/PhysRevLett.119.026404](https://doi.org/10.1103/PhysRevLett.119.026404)

Type-II Symmetry-Protected Topological Dirac Semimetals

Tay-Rong Chang^{*,1,2} Su-Yang Xu^{*†,3} Daniel S. Sanchez,³ Wei-Feng Tsai,^{4,5} Shin-Ming Huang,⁶
Guoqing Chang,^{4,5} Chuang-Han Hsu,^{4,5} Guang Bian,³ Ilya Belopolski,³ Zhi-Ming Yu,^{7,8}
Shengyuan A. Yang,⁸ Titus Neupert,⁹ Horng-Tay Jeng,^{1,10} Hsin Lin^{†,4,5} and M. Zahid Hasan^{†3}

¹*Department of Physics, National Tsing Hua University, Hsinchu 30013, Taiwan*

²*Department of Physics, National Cheng Kung University, Tainan, 701, Taiwan*

³*Laboratory for Topological Quantum Matter and Spectroscopy (B7),*

Department of Physics, Princeton University, Princeton, New Jersey 08544, USA

⁴*Centre for Advanced 2D Materials and Graphene Research Centre*

National University of Singapore, 6 Science Drive 2, Singapore 117546

⁵*Department of Physics, National University of Singapore, 2 Science Drive 3, Singapore 117542*

⁶*Department of Physics, National Sun Yat-Sen University, Kaohsiung 804, Taiwan*

⁷*School of Physics, Beijing Institute of Technology, Beijing 100081, China*

⁸*Research Laboratory for Quantum Materials, Singapore University of Technology and Design, Singapore 487372, Singapore*

⁹*Department of Physics, University of Zurich, Winterthurerstrasse 190, CH-8057 Zurich, Switzerland*

¹⁰*Institute of Physics, Academia Sinica, Taipei 11529, Taiwan*

(Dated: May 22, 2017)

The recent proposal of the type-II Weyl semimetal state has attracted significant interest. In this paper, we propose the concept of the three-dimensional type-II Dirac fermion and theoretically identify this new symmetry-protected topological state in the large family of transition-metal icosagenides, MA_3 ($M=V, Nb, Ta$; $A=Al, Ga, In$). We show that the VA_3 family features a pair of strongly Lorentz-violating type-II Dirac nodes and that each Dirac node consists of four type-II Weyl nodes with chiral charge ± 1 via symmetry breaking. Furthermore, we predict the Landau level spectrum arising from the type-II Dirac fermions in VA_3 that is distinct from that of known Dirac/Weyl semimetals. We also show a topological phase transition from a type-II Dirac semimetal to a quadratic Weyl semimetal or a topological crystalline insulator via crystalline distortions.

The correspondence between condensed matter and high-energy physics has been a source of inspiration throughout the history of physics. Advancements in topological band theory have uncovered a new and profound relations that has enabled the realization of elementary relativistic fermions in crystals with unique topologically non-trivial properties [1–20]. Specifically, the low-energy quasiparticle excitations of type-I Dirac semimetals [5–10], type-I Weyl semimetals [11–17], and topological superconductors [18–20] are the direct representations of relativistic Dirac, Weyl, and Majorana fermions, respectively. From an application perspective, what makes this realized connection with high-energy physics of importance and interest is the resulting broad range of topologically protected phenomena that can be potentially used for low-power electronics, spintronics, and robust qubits [21–23]. For these reasons, the type-I Dirac semimetal state in Na_3Bi [6, 7] and Cd_3As_2 [8, 9], the type-I Weyl semimetal state in the TaAs family of crystals [15, 17], and the various topological superconductor candidates [18–20] have attracted tremendous interest. Very recently, a new line of thinking that looks for new topological quasiparticles beyond direct analogs in

high-energy physics, has gained attention. Such an idea offers inroads into new topological phenomena that are not limited by the stringent constraints in high-energy physics [24–26]. A particularly interesting proposal is the prediction of type-II emergent Weyl fermions [27]. Type-I Weyl fermions, which have been realized in the TaAs family of crystals, are the direct analogs of the massless relativistic Weyl fermion from high-energy. They respect Lorentz symmetry and have the typical conical dispersion. In contrast, type-II Weyl fermions are dramatically Lorentz symmetry breaking, which is manifest in a tilted-over cone in energy-momentum space [27]. These Lorentz violating Weyl fermions can give rise to many new properties, such as a direction-dependent chiral anomaly [28], an anti-chiral effect of the chiral Landau level [29], novel quantum oscillations due to momentum space Klein tunneling [30], and a modified anomalous Hall conductivity [31]. The novel type-II Weyl semimetal state has been recently predicted/confirmed in a number of 3D crystals [27, 32–40].

Since the type-II behavior only relies on the fact that Lorentz invariance is not a necessary symmetry requirement in condensed matter physics, in solid-state crystals, Lorentz symmetry breaking is not limited to the type-II Weyl fermion and, in principle, can emerge in other particles, including the Weyl fermion’s most closely related particle, the Dirac fermion. However, to date, three-dimensional (3D) type-II Dirac fermions remain entirely lacking. In this letter, we propose the concept of the 3D

*These authors contributed equally to this work.

†Corresponding authors (emails): suyangxu@mit.edu, nilnish@gmail.com, mzhassan@princeton.edu

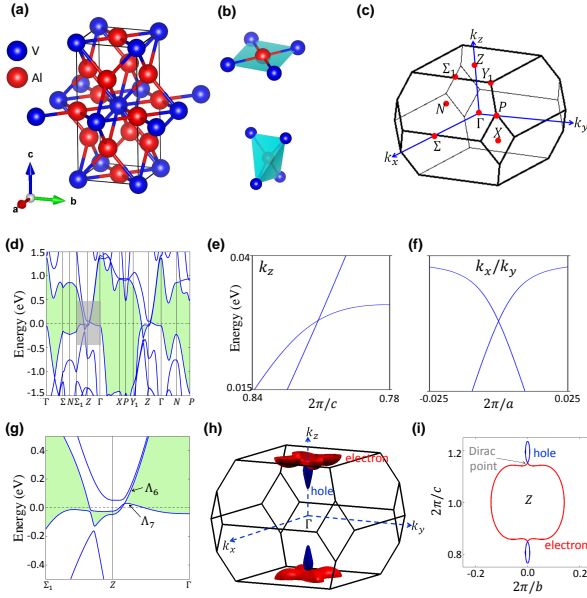


FIG. 1: (a) The Crystal structure of VAL_3 . The blue and red spheres representing the V and Al atoms, respectively. (b) The local structure of VAL_3 . (c) The bulk Brillouin zone (BZ) of VAL_3 . (d) The calculated bulk band structure of VAL_3 in the presence of spin-orbit coupling. The green shaded region shows the energy gap between the lowest conduction and valence bands. (e) A zoomed-in calculation of the band dispersion along the k_z and (f) k_x/k_y directions in the vicinity of the type-II Dirac node. (g) A zoomed-in view of the area highlighted by the gray box in (d). (h) Bulk Fermi surface of VAL_3 with the red and blue pockets denoting the electron and hole bands, respectively. (i) Bulk constant energy contour in (k_y, k_z) space at $k_x = 0$ and at the energy of the type-II Weyl nodes.

type-II Dirac semimetal state and identify it in a large family of transition-metal icosagenides, MA_3 ($\text{M}=\text{V}, \text{Nb}, \text{Ta}$; $\text{A}=\text{Al}, \text{Ga}, \text{In}$).

The VAL_3 family of compounds crystallizes in a body-centered tetragonal Bravais lattice with lattice constants $a = 3.78 \text{ \AA}$ and $c = 8.322 \text{ \AA}$ [41] and the space group $I4/mmm$ (No. 139), as shown in Fig. 1(a). In this structure, each Al atom is surrounded by four V atoms in two different local structures: a planer square and a tetrahedron geometry (Fig. 1(b)). Figure 1(c) shows the bulk Brillouin zone of the VAL_3 crystal.

We now present the calculated band structure of VAL_3 to reveal the Dirac node and its type-II character. The first-principles calculations was implemented in the VASP [42] package. A $15 \times 15 \times 15$ MonkhorstPack k -point mesh was used in the computations with a cutoff energy of 500 eV. The SOC effects were included in calculations self-consistently [43]. The calculated bulk band structure along high symmetry directions (Fig. 1(d)) reveal the semimetallic ground state. The zoomed-in view of the band structure (In Fig. 1(g)) shows, the conduction and valence bands cross each other along the $\Gamma - Z$

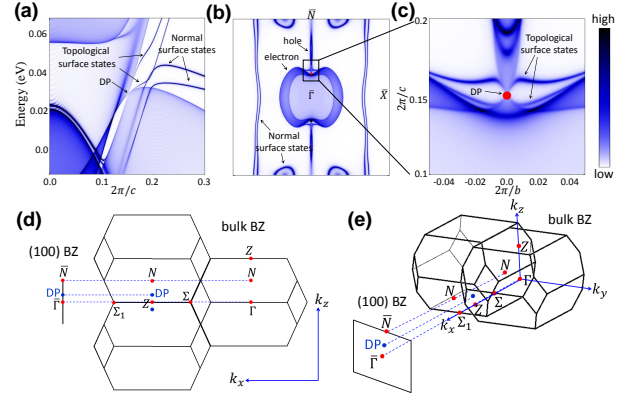


FIG. 2: (a) Surface and bulk band structure of VAL_3 along $\bar{\Gamma}-\bar{N}$ direction on the (100) surface BZ. (b) The calculated k_z - k_y surface and bulk electronic structure at the energy of the bulk Dirac node ($\sim 28 \text{ meV}$ above E_F). (c) Zoomed-in view of the area highlighted by the black box that surrounds the projected type-II Dirac node in (b). (d) The bulk BZ is projected onto the (100) surface form (k_x, k_z) side view and (e) tilted of view.

direction, forming a Dirac node near the Z point. Figures 1(e,f) show the energy dispersion away from the Dirac node along all three k directions. While the two bands have Fermi velocities of opposite signs along k_x and k_y directions, they have velocities of the same sign along k_z . Moreover, the constant energy contour at the energy of the Dirac node consists of an electron pocket and a hole pocket touching at the Dirac node (Fig. 1(i)). These observations demonstrate the first type-II Dirac fermion semimetal state.

In order to understand the topological properties of the type-II Dirac semimetal state in VAL_3 , we calculate the 2D \mathbb{Z}_2 invariant ν_{2D} and the mirror Chern number $n_{\mathcal{M}}$. Our calculations show that both the $k_z = 0$ and $k_z = \pi$ planes have a trivial \mathbb{Z}_2 number ($\nu_{k_z=0} = \nu_{k_z=\pi} = 0$) and that the $k_z = 0$ plane has a nontrivial mirror Chern number $n_{\mathcal{M}} = 2$. We note that existing Dirac semimetals Na_3Bi and Cd_3As_2 are known to possess a 2D \mathbb{Z}_2 ($\nu_{2D} = 1$) and a mirror Chern number ($n_{\mathcal{M}} = 1$), respectively [10]. Therefore, the result $n_{\mathcal{M}} = 2$ indicates that the Dirac semimetal state in VAL_3 is topologically distinct from that of in Cd_3As_2 or Na_3Bi [10]. We wish to note that the type-I/type-II property of the Dirac fermions is unrelated to the mirror Chern number, since the Dirac nodes are located at finite k_z values, whereas the mirror Chern number is defined on the $k_z = 0$ plane. Mathematically, theory allows a type-I Dirac semimetal to have a mirror Chern number $n_{\mathcal{M}} = 2$, but this type of system has not been found in real materials.

We now explore the existence of protected surface states in VAL_3 and their connection to the type-II Dirac nodes. In order to do so, we calculate the surface electronic structure of the (100) surface, where the two Dirac

nodes are projected onto different k locations in the surface BZ. Figures 2(d,e) show how the bulk BZ is projected onto the (100) surface. Due to the body-centered structural property, VAL_3 's (100) surface BZ center $\bar{\Gamma}$ corresponds to the projection of both the $\Sigma - \Gamma$ line and the $\Sigma_1 - Z$ line. Because the Dirac nodes are near the Z point in the bulk, their surface projections are close to the $\bar{\Gamma}$ point. Figure 2(a) shows the energy dispersion of surface band structure along the $\bar{\Gamma} - \bar{N}$ (k_z) direction. We observe surface states that emerge out of the Dirac node at $k_z \simeq 0.15 \frac{2\pi}{c}$, suggesting the existence of Fermi arcs. In Figs. 2(b,c), we present the surface constant energy contour at the energy of the bulk Dirac node. We see two pairs of Fermi arcs terminated onto a Dirac node. They start from the Dirac node and quickly merge onto the projected electron-like pocket.

To further showcase the novel physics that may be studied in VAL_3 , we will now turn our attention towards investigating its topological phase transitions. Generically, a Dirac semimetal can be regarded as a critical point of different phases. In Fig. 3(e) we show a cartoon illustration of the (100) surface Fermi surface of VAL_3 . Interestingly, the mirror Chern number $n_{\mathcal{M}} = 2$ defined on the $k_z = 0$ plane and the number of Fermi arcs found at each Dirac node are consistent with each other. We first show the topological phase transition from the type-II Dirac semimetal state to a topological crystalline insulator state. We break the C_{4z} rotational symmetry by compressing the lattice along the \hat{x} direction which makes $a \neq b$, for example, by applying external pressure along the (100) or (010) direction. This opens up a gap at VAL_3 's type-II Dirac nodes. Because of $n_{\mathcal{M}} = 2$ at $k_z = 0$, the resulting insulating phase is a topological crystalline insulator with two Dirac surface states as shown in Fig. 3(d). We now show two consecutive topological phase transitions which transform the type-II Dirac fermions first to quadratic double Weyl fermions with chiral charge ± 2 then to linear single Weyl fermions with chiral charge ± 1 . As shown in Figs. 3(e-g), we apply a Zeeman field along the k_z direction. This field breaks time-reversal symmetry but preserves the C_4 rotational symmetry. As a result, each type-II Dirac node is found to split into a pair of quadratic Weyl nodes with chiral charge of ± 2 . Because of the ± 2 chiral charge, each quadratic Weyl node is required to have two Fermi arcs. Interestingly, the four Fermi arcs associated with each Dirac node naturally provide the Fermi arcs needed for the pair of quadratic Weyl nodes. Since the C_4 rotational symmetry is preserved, the quadratic Weyl nodes are still along the C_4 rotational (k_z) axis. The k space distribution of the quadratic Weyl nodes (Fig. 3(f)) breaks time-reversal symmetry. As a result, as shown in Fig. 3(f), any (k_x, k_y) slice whose k_z is between the immediate pair of quadratic Weyl nodes has a Chern number of 2. The fact that the BZ carries nonzero chiral number suggests the existence of anomalous Hall current σ_{xy} that arises

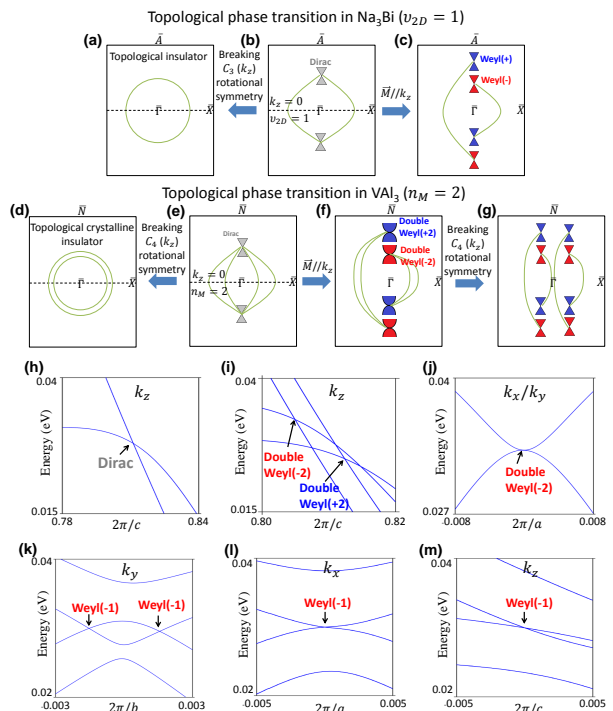


FIG. 3: (a-c) A schematic of the the phase transition and corresponding Fermi surface in Na_3Bi . (a) A topological insulating phase by breaking the C_{3z} rotational symmetry. (c) A single Weyl phase by applying a Zeeman field along the rotational symmetry preserving axis. (d-g) Schematic illustration of the topological phase transitions and corresponding Fermi surface in VAL_3 . (d) A topological crystalline insulator phase by breaking the C_{4z} rotational symmetry. (e) An illustration of surface Fermi arcs and type-II Dirac nodes. (f) Type-II Dirac node splits into a pair of double Weyl nodes with chiral charge ± 2 by applying a Zeeman field along the k_z -axis. (g) By further applying a C_{4z} symmetry breaking perturbation, each double Weyl nodes split into two single Weyl nodes with ± 1 chiral charge. The net Chern number for the regions defined by dashed lines is shown. (h-m) The calculated band dispersion in different topological phase in VAL_3 . The band dispersion along the k_z directions without (h) and with Zeeman field (i). (j) The band dispersion along the k_x/k_y direction for the type-II double Weyl cone in panel (i). (k) By breaking the C_{4z} symmetry, the double Weyl node in panel (j) splits into two single Weyl nodes with an equal chiral charge of -1 . (l) The zoomed-in band dispersions along k_x and (m) k_z directions for the single Weyl nodes.

from the quadratic Weyl nodes [52]. Figure 3(i) shows the calculated band structure along k_z in the presence of the Zeeman field, where we see that the type-II Dirac fermion (Fig. 3(h)) indeed splits into a pair of type-II quadratic Weyl nodes. Each quadratic Weyl fermion disperses quadratically along k_x and k_y directions (Fig. 3(j)) but linearly along k_z direction (Fig. 3(i)). Experimentally, a Zeeman field can be achieved by inducing ferromagnetism via doping magnetic elements, as achieved in other semiconductors and semimetals [53–56]. Here we

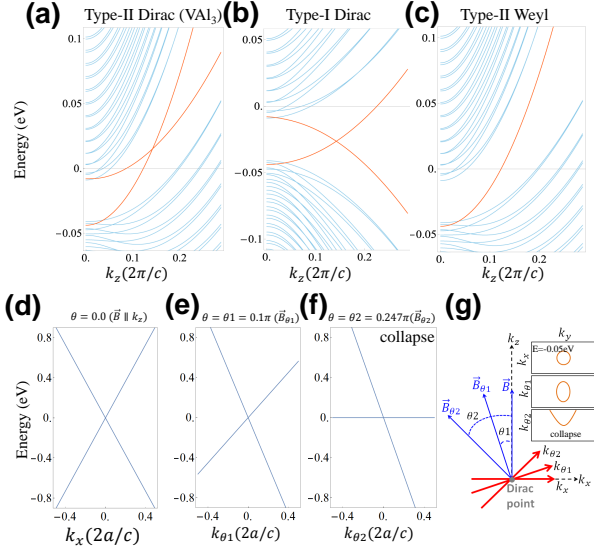


FIG. 4: (a) Landau level spectrum of the type-II Dirac fermions in VA1_3 . The magnetic field is along the tilting direction of the type-II Dirac fermions, which is the k_z direction for VA1_3 . (b) Landau level spectrum of the type-I Dirac fermions and (c) type-II Weyl fermions. (d-f) The band dispersion with Varying the magnetic field direction within the (k_x, k_z) plane. θ defines the angle between the magnetic field and k_z shown in panel (g). (d) The band dispersion along k_x . (e) The band dispersion along $k_{\theta 1}$. (f) The band dispersion along $k_{\theta 2}$. (g) Schematic illustration of different magnetic field directions and also the k directions $(k_x, k_{\theta 1}, k_{\theta 2})$ that are perpendicular to the magnetic fields. The three insets on the top-right corner shows the constant energy contours in the k plane that is perpendicular to the magnetic field.

propose to dope Cr into VA1_3 to induce ferrimagnetism. In Figs. 3(g), we further break the C_4 rotational symmetry. We find that the C_4 breaking splits each double Weyl nodes with chiral charge ± 2 into two single Weyl node with chiral charge ± 1 . Therefore, a net number of four Weyl nodes are generated from a single type-II Dirac node in VA1_3 . Depending on whether one compresses the lattice along \hat{x} or \hat{y} direction, the splitting of the double Weyl nodes will be along k_x or k_y direction. Figure 3(k-m) show the situation where the lattice was compressed along the \hat{x} direction. We see that each quadric Weyl node split into two single Weyl nodes along k_y direction.

Finally, we study the Landau band (LB) spectrum of the type-II Dirac fermions in VA1_3 (Fig. 4), which plays a key role in the magneto-transport properties of materials. We first compare the LB spectra of Weyl fermion, type-I Dirac fermion and type-II Dirac fermion. The lowest LB of a Weyl fermion is a chiral band (Fig. 4(c)), whereas the lowest LBs of a Dirac fermion consist of a pair of counter-propagating chiral bands (Fig. 4(a,b)) whose Fermi velocities are of the opposite (same) sign if the Dirac fermions are of type-I(II). One can measure the SdH quantum oscillations [57] or the quantum oscil-

lations of magnetic torque [58]. The lowest Landau level can be accessed at high magnetic fields. Since the band structures of the lowest LLs of a Dirac cone, a Weyl cone and a parabolic band are distinctly different, it is expected to manifest in the transport signals. We find that the type-II character in VA1_3 leads to a distinct response in its Landau level spectrum, i.e., the existence of a critical angle of the magnetic field, along which all Landau levels “collapse” into the same energy, giving rise to a large density of states [29, 30]. We start from the condition where the magnetic field is parallel to the tilting direction of the type-II Dirac cone, i.e., the k_z direction in VA1_3 . In this case, the electrons’ cyclotron motions are within the (k_x, k_y) plane. In the semiclassical picture, the electrons will trace the Fermi contour within this plane. Fig. 4(d) shows the band dispersion along k_x . Since the dispersion has a typical conical shape, the constant energy contour is a closed loop independent of the chemical potential position (the top panel of inset of Fig. 4(g)). We now vary the magnetic field direction within the (k_x, k_z) plane. Figure 4(e) shows the energy dispersion along $k_{\theta 1}$ that is perpendicular to the magnetic field $B_{\theta 1}$ in Fig. 4(g). We see that the dispersion becomes a tilted cone, while the constant energy contour is a still closed loop (the middle panel of inset of Fig. 4(g)). As we continue to tilt the magnetic field, there exists a critical angle, at which one of the bands becomes flat. This means that, to the lowest order (k^1 term in the $k \cdot p$ theory [43].), the Fermi contour becomes non-closed (the bottom panel of inset of Fig. 4(g)). Interestingly, our calculations show that, to the lowest order, all Landau levels collapse to the same energy, leading to a large density of states (Fig. 4(f)). This can be seen in the angle-dependent magneto-transport experiments. Based on the calculated band structure of VA1_3 , we obtain a critical angle 0.247π (between the magnetic field and k_z) for the type-II Dirac fermions in VA1_3 . The Landau level spectra with different magnitudes of the Zeeman field are shown in the Supplementary Material [43].

In summary, we have theoretically identified the type-II Dirac fermion semimetal state in the VA1_3 family of materials. Distinct from a type-I Dirac semimetal such as Cd_3As_2 and Na_3Bi , the Dirac node in VA1_3 splits into four type-II Weyl nodes under symmetry breaking. The type-II Dirac fermions, the Fermi arc surface states, the topological phase transitions and the distinct LB spectrum in VA1_3 suggest many interesting topological phenomena that can be measured in electrical transport, optical transport, and scanning tunneling spectroscopic experiments.

T.-R.C. and H.-T.J. are supported by the Ministry of Science and Technology, the National Tsing Hua University, the National Cheng Kung University, and the Academia Sinica, Taiwan. T.-R.C. and H.-T.J. also thank the National Center for High-performance Computing, the Computer and Information Network-

ing Center-National Taiwan University, and the National Center for Theoretical Sciences, Taiwan for technical support. S.-M.H is supported by the Ministry of Science and Technology in Taiwan under Grant No. MOST105-2112-M-110-014-MY3. Work at the National University of Singapore is supported by the National Research Foundation (NRF), Prime Ministers Office, Singapore, under its NRF fellowship (NRF award no. NRF-NRFF2013-03). Work at Singapore University of Technology and Design is supported by Singapore MOE Academic Research Fund Tier 2 (MOE2015-T2-2-144). Work at Princeton University is supported by the U.S. Department of Energy (DOE), Office of Science, Basic Energy Sciences (BES) under the grant number DE-FG-02-05ER46200.

-
- [1] C. Herring, *Phys. Rev.* **52**, 365 (1937).
 [2] H. Weyl, *Z. Phys.* **56**, 330 (1929).
 [3] A. M. Turner and A. Vishwanath, arXiv:1301.0330 (2013).
 [4] M. Z. Hasan, S.-Y. Xu, and M. Neupane, in *Topological Insulators: Fundamentals and Perspectives* edited by F. Ortmann, S. Roche, S. O. Valenzuela (John Wiley & Sons, 2015).
 [5] Z. Wang, Y. Sun, X.-Q. Chen, C. Franchini, G. Xu, H. Weng, X. Dai, and Z. Fang, *Phys. Rev. B* **85**, 195320 (2012).
 [6] Z. K. Liu, B. Zhou, Y. Zhang, Z. J. Wang, H. M. Weng, D. Prabhakaran, S.-K. Mo, Z. X. Shen, Z. Fang, X. Dai, Z. Hussain, and Y. L. Chen, *Science* **343**, 864 (2014).
 [7] S.-Y. Xu, C. Liu, S. K. Kushwaha, R. Sankar, J. W. Krizan, I. Belopolski, M. Neupane, G. Bian, N. Alidoust, T.-R. Chang, H.-T. Jeng, C.-Y. Huang, W.-F. Tsai, H. Lin, P. P. Shibayev, F.-C. Chou, R. J. Cava, and M. Z. Hasan, *Science* **347**, 294 (2015).
 [8] M. Neupane, S.-Y. Xu, R. Sankar, N. Alidoust, G. Bian, C. Liu, I. Belopolski, T.-R. Chang, H.-T. Jeng, H. Lin, A. Bansil, F. Chou, and M. Z. Hasan, *Nature Commun.* **5**, 3786 (2014).
 [9] S. Borisenko, Q. Gibson, D. Evtushinsky, V. Zabolotnyy, B. Büchner, and R. J. Cava, *Phys. Rev. Lett.* **113**, 027603 (2014).
 [10] B.-J. Yang and N. Nagaosa, *Nature Commun.* **5**, 4898 (2014).
 [11] X. Wan, A. M. Turner, A. Vishwanath, and S. Y. Savrasov, *Phys. Rev. B* **83**, 205101 (2011).
 [12] A. A. Burkov and L. Balents, *Phys. Rev. Lett.* **107**, 127205 (2011).
 [13] S.-M. Huang, S.-Y. Xu, I. Belopolski, C.-C. Lee, G. Chang, B. Wang, N. Alidoust, G. Bian, M. Neupane, C. Zhang, S. Jia, A. Bansil, H. Lin, and M. Z. Hasan, *Nature Commun.* **6**, 7373 (2015).
 [14] H. Weng, C. Fang, Z. Fang, B. A. Bernevig, and X. Dai, *Phys. Rev. X* **5**, 011029 (2015).
 [15] S.-Y. Xu, I. Belopolski, N. Alidoust, M. Neupane, G. Bian, C. Zhang, R. Sankar, G. Chang, Z. Yuan, C.-C. Lee, S.-M. Huang, H. Zheng, J. Ma, D. S. Sanchez, B. Wang, A. Bansil, F. Chou, P. P. Shibayev, H. Lin, S. Jia, and M. Z. Hasan, *Science* **349**, 613 (2015).
 [16] L. Lu, Z. Wang, D. Ye, L. Ran, L. Fu, J. D. Joannopoulos, and M. Soljačić, *Science* **349**, 622 (2015).
 [17] B. Q. Lv, H. M. Weng, B. B. Fu, X. P. Wang, H. Miao, J. Ma, P. Richard, X. C. Huang, L. X. Zhao, G. F. Chen, Z. Fang, X. Dai, T. Qian, and H. Ding, *Phys. Rev. X* **5**, 031013 (2015).
 [18] V. Mourik, K. Zuo, S. M. Frolov, S. R. Plissard, E. P. A. M. Bakkers, and L. P. Kouwenhoven, *Science* **336**, 1003-1007 (2012).
 [19] J.-P. Xu, M.-X. Wang, Z. L. Liu, J.-F. Ge, X. Yang, C. Liu, Z. A. Xu, D. Guan, C. L. Gao, D. Qian, Y. Liu, Q.-H. Wang, F.-C. Zhang, Q.-K. Xue, and J.-F. Jia, *Phys. Rev. Lett.* **114**, 017001 (2015).
 [20] K. Matano, M. Kriener, K. Segawa, Y. Ando, and G.-q. Zheng, *Nature Phys.* **12**, 852 (2016).
 [21] S. A. Parameswaran, T. Grover, D. A. Abanin, D. A. Pesin, and A. Vishwanath, *Phys. Rev. X* **4**, 031035 (2014).
 [22] X. Huang, L. Zhao, Y. Long, P. Wang, D. Chen, Z. Yang, H. Liang, M. Xue, H. Weng, Z. Fang, X. Dai, and G. Chen *Phys. Rev. X* **5**, 031023 (2015).
 [23] C.-L. Zhang, S.-Y. Xu, I. Belopolski, Z. Yuan, Z. Lin, B. Tong, G. Bian, N. Alidoust, C.-C. Lee, S.-M. Huang, T.-R. Chang, G. Chang, C.-H. Hsu, H.-T. Jeng, M. Neupane, D. S. Sanchez, H. Zheng, J. Wang, H. Lin, C. Zhang, H.-Z. Lu, S.-Q. Shen, T. Neupert, M. Z. Hasan, and S. Jia, *Nature Commun.* **7**, 10735 (2016).
 [24] A. G. Grushin, *Phys. Rev. D* **86**, 045001 (2012).
 [25] E. J. Bergholtz, Z. Liu, M. Trescher, R. Moessner, and M. Udagawa, *Phys. Rev. Lett.* **114**, 016806 (2015).
 [26] M. Trescher, B. Sbierski, P. W. Brouwer, and E. J. Bergholtz, *Phys. Rev. B* **91**, 115135 (2015).
 [27] A. A. Soluyanov, D. Gresch, Z. Wang, Q. Wu, M. Troyer, X. Dai, and B. A. Bernevig, *Nature* **527**, 495 (2015).
 [28] M. Udagawa, and E.J. Bergholtz, *Phys. Rev. Lett.* **117**, 086401 (2016).
 [29] Z.-M. Yu, Y. Yao, and S. A. Yang, *Phys. Rev. Lett.* **117**, 077202 (2016).
 [30] T. E. O'Brien, M. Diez, and C. W. J. Beenakker, *Phys. Rev. Lett.* **116**, 236401 (2016).
 [31] A. A. Zyuzin and R. P. Tiwari, *JETP Lett.* **103**, 717 (2016).
 [32] Y. Sun, S.-C. Wu, M. N. Ali, C. Felser, and B. Yan, *Phys. Rev. B* **92**, 161107 (2015).
 [33] T.-R. Chang, S.-Y. Xu, G. Chang, C.-C. Lee, S.-M. Huang, B. Wang, G. Bian, H. Zheng, D. S. Sanchez, I. Belopolski, N. Alidoust, M. Neupane, A. Bansil, H.-T. Jeng, H. Lin, and M. Z. Hasan, *Nature Commun.* **7**, 10639 (2016).
 [34] Z. Wang, D. Gresch, A. A. Soluyanov, W. Xie, S. Kushwaha, X. Dai, M. Troyer, R. J. Cava, and B. A. Bernevig, *Phys. Rev. Lett.* **117**, 056805 (2016).
 [35] S.-Y. Xu, N. Alidoust, G. Chang, H. Lu, B. Singh, I. Belopolski, D. Sanchez, X. Zhang, G. Bian, H. Zheng, M.-A. Hsuan, Y. Bian, S.-M. Huang, C.-H. Hsu, T.-R. Chang, H.-T. Jeng, A. Bansil, V. N. Strocov, H. Lin, S. Jia, and M. Z. Hasan, arXiv:1603.07318 (2016).
 [36] G. Chang, S.-Y. Xu, D. S. Sanchez, S.-M. Huang, C.-C. Lee, T.-R. Chang, H. Zheng, G. Bian, I. Belopolski, N. Alidoust, H.-T. Jeng, A. Bansil, H. Lin, and M. Z. Hasan, *Science Advances*, **2**, e1600295 (2016).
 [37] K. Koepnick, D. Kasinathan, D. V. Efremov, S. Khim, S. Borisenko, B. Büchner, and J. van den Brink, *Phys. Rev. B* **93**, 201101(R) (2016)

- [38] I. Belopolski, S.-Y. Xu, Y. Ishida, X. Pan, P. Yu, D. S. Sanchez, H. Zheng, M. Neupane, N. Alidoust, G. Chang, T.-R. Chang, Y. Wu, G. Bian, S.-M. Huang, C.-C. Lee, D. Mou, L. Huang, Y. Song, B. Wang, G. Wang, Y.-W. Yeh, N. Yao, J. E. Rault, P. LeFèvre, F. Bertran, H.-T. Jeng, T. Kondo, A. Kaminski, H. Lin, Z. Liu, F. Song, S. Shin, and M. Z. Hasan, *Phys. Rev. B* **94**, 085127 (2016).
- [39] I. Belopolski, D. S. Sanchez, Y. Ishida, X. Pan, P. Yu, S.-Y. Xu, G. Chang, T.-R. Chang, H. Zheng, N. Alidoust, G. Bian, M. Neupane, S.-M. Huang, C.-C. Lee, Y. Song, H. Bu, G. Wang, S. Li, G. Eda, H.-T. Jeng, T. Kondo, H. Lin, Z. Liu, F. Song, S. Shin, and M. Z. Hasan, *Nature Commun.* **7**, 13643 (2016).
- [40] F. Y. Bruno, A. Tamai, Q. S. Wu, I. Cucchi, C. Barreteau, A. de la Torre, S. McKeown Walker, S. Riccò, Z. Wang, T. K. Kim, M. Hoesch, M. Shi, N. C. Plumb, E. Giannini, A. A. Soluyanov, and F. Baumberger, *Phys. Rev. B* **94**, 121112 (2016).
- [41] J. H. Maas, G. F. Bastin, F. J. J. van Loo, and R. Metselaar, *Zeitschrift für Metallkunde* **74** 294 (1983).
- [42] G. Kresse and J. Furthmüller, *Comput. Mater. Sci.* **6**, 15 (1996).
- [43] See Supplemental Material for the details of the calculation methods, $\mathbf{k} \cdot \mathbf{p}$ model, and the band structures of VAI_3 family, which includes Refs. [44–51].
- [44] P. E. Blöchl, *Phys. Rev. B* **50**, 17953-17979 (1994).
- [45] G. Kresse and D. Joubert, *Phys. Rev. B* **59**, 1758-1775 (1999).
- [46] J. P. Perdew, K. Burke, and M. Ernzerhof, *Phys. Rev. Lett.* **77**, 3865 (1996).
- [47] N. Marzari and D. Vanderbilt, *Phys. Rev. B* **56**, 12847 (1997).
- [48] I. Souza, N. Marzari, and D. Vanderbilt, *Phys. Rev. B* **65**, 035109 (2001).
- [49] A. A. Mostofi, J. R. Yates, Y.-S. Lee, I. Souza, D. Vanderbilt, and N. Marzari, *Comput. Phys. Commun.* **178**, 685-699 (2008).
- [50] C. Franchini, *J. Phys. Condens. Matter* **24**, 235602 (2012).
- [51] B.-J. Yang and N. Nagaosa, *Nature Commun.* **5**, 4898 (2014).
- [52] A. A. Burkov, *Phys. Rev. Lett.* **113**, 187202 (2014).
- [53] C.-Z. Chang, W. Zhao, D. Y. Kim, H. Zhang, B. A. Assaf, D. Heiman, S.-C. Zhang, C. Liu, M. H. W. Chan, and J. S. Moodera, *Nature mat.* **14**, 473 (2015).
- [54] Z. Wang, K. Segawa, S. Sasaki, A. A. Taskin, and Y. Ando, *APL Materials*, **3**, 083302 (2015)
- [55] P. P. J. Haazen, J.-B. Laloë, T. J. Nummy, H. J. M. Swagten, P. Jarillo-Herrero, D. Heiman, and J. S. Moodera, *Appl. Phys. Lett.* **100**, 082404 (2012).
- [56] S. Choia, G.-B. Chaa, S.C. Honga, S. Choa, Y. Kimb, J.B. Kettersonb, S.-Y. Jeongc, and G.-C. Yi, *Solid state commun.* **122**, 165 (2002).
- [57] C. Zhang, Z. Lin, C. Guo, S.-Y. Xu, C.-C. Lee, H. Lu, S.-M. Huang, G. Chang, C.-H. Hsu, H. Lin, L. Li, C. Zhang, T. Neupert, M. Z. Hasan, J. Wang, and S. Jia, *arXiv:1507.06301* (2015).
- [58] P. J.W. Moll, A. C. Potter, B. Ramshaw, K. Modic, S. Riggs, B. Zeng, N. J. Ghimire, E. D. Bauer, R. Kealhofer, N. Nair, F. Ronning, and J. G. Analytis, *Nature commun.* **7**, 12492 (2016).